A Letters Journal Exploring the Frontiers of Physics

July 2025

EPL, **151** (2025) 26002
doi: 10.1209/0295-5075/adec17

www.epljournal.org

Focus Article

Measurement of the unusual dielectric response to low-frequency s-polarized evanescent waves in metals with implications for the Casimir effect[(a)]

M. Dhital[1], G. L. Klimchitskaya[2,3], V. M. Mostepanenko[2,3] and U. Mohideen[1(b)]

[1] *Department of Physics and Astronomy, University of California - Riverside, CA 92521, USA*
[2] *Central Astronomical Observatory at Pulkovo of the Russian Academy of Sciences - Saint Petersburg, 196140, Russia*
[3] *Peter the Great Saint Petersburg Polytechnic University - Saint Petersburg, 195251, Russia*

received 15 May 2025; accepted in final form 4 July 2025
published online 12 August 2025

Abstract – We report precision measurements of the lateral component of the oscillating magnetic field reflected from a copper plate, which is fully determined by s-polarized evanescent waves. The measurement data are compared with theoretical predictions of classical electrodynamics using the dielectric permittivity of copper as given by the Drude model. It is shown that these predictions are excluded by the measurement data which means that the currently used Drude model does not provide a complete description of the electromagnetic response of metals for s-polarized evanescent waves. The critical importance of this result for several fields of condensed matter physics and optics dealing with evanescent waves, including the Casimir effect, is discussed.

Introduction. – Paul Drude proposed his model of electrical conduction of metals 125 years ago. After the necessary modifications taking into account quantum theory, which were made in 1933 by Arnold Sommerfeld, this model was extensively used for the description of an immense number of electrical phenomena in condensed matter physics, optics, and applied physics [1]. According to the Drude model, the frequency-dependent dielectric permittivity describing the response of metals to an alternating electromagnetic field is given by

$$\varepsilon(\omega)=1-\frac{\omega_p^2}{\omega[\omega+i\gamma(T)]}, \tag{1}$$

where ω_p is the plasma frequency and γ is the temperature-dependent relaxation parameter which is inverse of the mean free time for electron-ion collisions.

The dielectric permittivity (1) has an abundance of experimental confirmations in both classical and quantum physics as well as in electrical engineering. In 2003, it was, however, shown that the values of the Casimir force [2] between metallic surfaces calculated by the fundamental Lifshitz theory [3–5] using the permittivity (1) at low frequencies are excluded by the measurement data [6]. Currently the Casimir force finds extensive applications in both fundamental physics and nanotechnology (see the monographs [7–11] and reviews [12–16]. Like the van der Waals force, it is determined by quantum fluctuations of the electromagnetic field, but acts at larger separations between the interacting bodies, where the effects of relativistic retardation contribute to the result.

The experiment [6] was followed by experiments of increasing precision performed by means of a micromechanical torsional oscillator [17–21] and by an atomic force microscope [22–28]. These experiments used different preparation details of thin metallic (Au) layers and different measurement techniques, but no discrepancy in the obtained data was observed. In all these experiments, the predictions of the Lifshitz theory obtained using the permittivity of metals (1) were excluded by the measurement data. Thus, in the differential force measurement [20],

[(a)] Contribution to the *Focus Issue on Casimir Effect and Its Role in Modern Physics* edited by Galina L. Klimchitskaya and Vladimir M. Mostepanenko.
[(b)] E-mail: umar@ucr.edu (corresponding author)

the difference between the theoretical results and the experimental data was confirmed by up to a factor of 1000. The limitations of the permittivity (1) for a description of the low-frequency electromagnetic response of Au in calculations of the Casimir force were confirmed up to separations of 1.1μm [28] and 4.8μm [21] between the interacting surfaces. It was shown [29] that taking into account the dependence of the relaxation parameter in eq. (1) on the frequency (the so-called Gurzhi model) does not bring the theoretical predictions in the above experiments into agreement with the measurement data. Only one measurement of the Casimir force at large separations stated that the data are in agreement with theory using the Drude model [30], but this conclusion was reached by omitting the background force of unknown origin which exceeded the Casimir force by an order of magnitude and disregarding the role of imperfections on the surface of a glass lens of centimeter-size radius [31,32].

According to the Lifshitz formula for the Casimir force written along the real frequency axis, both the propagating (on-the-mass-shell, where for the photon frequency and momentum equation $\omega = kc$ holds) and evanescent (off-the-mass-shell, where $\omega \neq kc$) waves of both s- and p-polarizations contribute to the result. These contributions were analyzed by several authors [33–37]. It is now well established [38] that the difference between theoretical predictions and the measurement data is completely determined by the contribution of the s-polarized (transverse electric) evanescent waves.

It should be noted that most of experimental confirmations of the permittivity (1) fall in the region of propagating waves. Physics of surface plasmon polaritons [39,40] provides a lot of data regarding the response of metals to the evanescent waves, but for only the p-polarized case. The same is true regarding near-field optical microscopy [41–44] used to surpass the standard resolution limit. Regarding the phenomena of total internal reflection and frustrated total internal reflection [45–47], they allow testing the response of metals to electromagnetic waves with very small deviations from the mass-shell equation. This means that in the region of strongly evanescent s-polarized waves the dielectric permittivity (1) has not been experimentally confirmed.

As a potential test, an experiment sensitive to the reflection coefficient for s-polarization in the range of strongly evanescent waves has been proposed [48,49] which uses an oscillating magnetic dipole placed at height h above a thick metallic plate. It was shown that the lateral component of emitted magnetic field observed at the height $z = h$ at a sufficiently large distance x from the dipole is completely determined by the s-polarized evanescent waves. Thus, it is possible to directly test the model of the electromagnetic response of a metal to the s-polarized evanescent waves by comparing the theoretical results with measurement data.

In this letter, we experimentally probe the response of metals to the low-frequency s-polarized evanescent waves by measuring the magnitude of lateral component of the magnetic field reflected from a copper surface. According to our results, the theoretical values of the reflected field component computed at different separations from the emitter using the dielectric permittivity (1) do not provide an accurate description of the measurement data. Possible implications of this result in the Casimir effect and, more widely, in several areas of condensed matter physics and optics dealing with evanescent waves are discussed.

Configuration. – We consider the electromagnetic field emitted by a coil (magnetic dipole) spaced at the height $z = h$ above the coordinate origin $x = 0$, $y = 0$ on a thick metallic plate characterized by the dielectric permittivity $\varepsilon(\omega)$. The magnetic moment of this dipole oscillates with the frequency ω_d and is directed along the z-axis,

$$\mathbf{m} = (0, 0, m_0 e^{-i\omega_d t}). \tag{2}$$

It is assumed that the dipole size is much less than h, the separation distance r between the dipole and the observation point of the emitted field, and the wavelength $\lambda_d = 2\pi c/\omega_d$. It is also assumed that $r \ll \lambda_d$. As a result, the components of the electric field at the observation point are smaller than those of the magnetic field by the factor of $\lambda_d/(2\pi r) \sim 10^9$ [48–50].

Under these conditions, the x-component of the magnetic field at a point (x, y, z) separated from the dipole by the distance $r = [x^2 + y^2 + (z-h)^2]^{1/2}$ is given by [48,49]

$$B_x(\omega_d, r) = \frac{\mu_0 m_0 x}{4\pi}\left[\frac{1}{\rho}\int_{\omega_d/c}^{\infty} \mathrm{d}k_\perp k_\perp^2 J_1(k_\perp\rho) R_\mathrm{s}(\omega_d, k_\perp) \times e^{-q(z+h)} - \frac{z-h}{r^2}\left(\frac{\omega_d^2}{c^2 r} + 3i\frac{\omega_d}{cr^2} - \frac{3}{r^3}\right) e^{i\frac{\omega_d}{c}r}\right], \tag{3}$$

where $\rho = (x^2 + y^2)^{1/2}$, $q^2 = k_\perp^2 - \omega_d^2/c^2$, and $k_\perp$ is the magnitude of the wave vector projection on the plane of metallic plate, $J_1(z)$ is the Bessel function, and μ_0 is the magnetic permeability of vacuum. The reflection coefficient on a metallic plate of sufficiently large thickness D for the s-polarized electromagnetic waves is defined as [10]

$$R_\mathrm{s}(\omega_d, k_\perp) = \frac{q^2 - p^2}{q^2 + p^2 + 2qp\coth(pD)}, \tag{4}$$

where $p^2 = k_\perp^2 - \varepsilon(\omega_d)\omega_d^2/c^2$. The component $B_y(\omega_d, r)$ of the magnetic field is obtained from eq. (3) by the replacement $x \to y$. Note that all fields here and below depend on t as $\exp(-i\omega_d t)$.

As is seen in eq. (3), the reflected magnetic field from the plate is fully determined by the evanescent waves. According to the results of [48,49], the contribution of the propagating waves to the reflected magnetic field is a factor of $\lambda_d^3/(2\pi r)^3 \sim 10^{27}$ smaller than that of the evanescent waves.

Experimental setup. – The experimental setup, shown in fig. 1, involves two coils (magnetic dipoles): one for generating the low-frequency magnetic field (emitter)

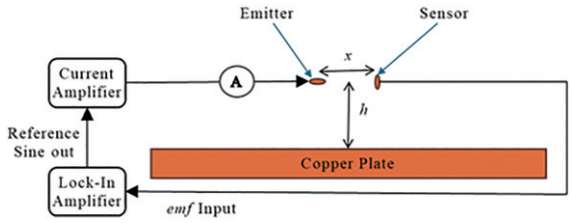

Fig. 1: Schematic of the experimental setup. Picture not to scale. The Lock-In Amplifier supplies the sinusoidal reference signal at the desired frequency as well as measures the amplitude and phase of the emf generated in the sensor coil from the lateral component of the reflected magnetic field. The emf measured is calibrated to the magnetic field as discussed in the text. The current from the Current Amplifier is measured using the ammeter shown as A. The emitter was cooled by blowing dry liquid nitrogen vapor to allow the use of large currents.

and the second for measuring the reflected magnetic field from a copper plate (sensor). An AC current was applied to the first coil, *i.e.*, "emitter," to produce the oscillating magnetic field. This field was then reflected by a $D = 2.5\,\mathrm{cm}$ thick copper plate ($30\times30\,\mathrm{cm}^2$ area), placed at a distance h mm below the emitter. The second coil, *i.e.*, "sensor," was placed at a fixed distance of x mm from the emitter and at the same height h above the copper plate to detect the reflected magnetic field. The distances were measured from the centers of the coils to the top surface of the plate. The emitter coil axis and the copper plate surface were oriented perpendicular to each other, while the sensor coil axis was perpendicular to the emitter axis and parallel to the copper plate surface.

Most often, the test bodies used in precision measurements of the Casimir force between metals were made of gold [17–22,26–28]. Gold is the suitable material primarily because its chemical inactivity which allows the surface properties to be stable during the experiment. In addition, gold also has the beneficial property of very high electric conductivity and associated excellent optical reflectivity. In this experiment, the copper plate was used as the model material for the following reasons. First, a material with very high electrical conductivity is needed. High chemical purity copper (used here) has 30% higher electrical conductivity than gold. Second, if there are deviations from the theory using the Drude and plasma models, they would be most strongly exhibited at low frequencies below 100 Hz, where the large plate thickness on the few cm scale is needed based on the large skin depth. In doing so, the area has to be at least $30\times30\,\mathrm{cm}^2$ for the h and x distances needed. A high purity gold plate with such dimensions would be prohibitively expensive. For these two reasons, the gold plate was not used in this experiment. In addition one should not expect big discrepancy in the measurement results obtained for different good conductors.

The coordinates of the emitter and sensor centers in the experimental configuration are $(0,0,h)$ and $(x,0,h)$, respectively. Then, according to eq. (3), the lateral component of the magnetic field at the observation point is completely determined by the part reflected from the plate,

$$B_x(\omega_d,x)=\frac{\mu_0 m_0}{4\pi}\int_{\omega_d/c}^{\infty}\mathrm{d}k_\perp k_\perp^2 J_1(k_\perp x)R_{\mathrm{s}}(\omega_d,k_\perp)e^{-2hq}, \tag{5}$$

whereas $B_y=0$.

The first and most crucial step in this experiment is to create the appropriate magnetic dipoles for the generation of the magnetic field with the emitter coil as well as the measurement of the lateral component of the reflected magnetic field with the sensor coil. The challenge in creating an appropriate magnetic dipole for the magnetic field generation is that it must approximate a point dipole in comparison to the other dimensions x and h in the setup. This means that the radius of the coil should be physically much less than x and h while still be capable of generating a sufficiently strong magnetic field that can be detected after reflecting off a metal plate placed at large x and h. Therefore, the coil needs to be rather small in size while being capable of handling large currents greater than $I = 1$ A to generate the required stronger magnetic fields. A second challenge is designing a sensor coil again of very small size similar to the emitter but that can detect extremely weak magnetic fields (on the nT scale) reflected from the copper plate at large distances compared to the size of the coil.

Two different copper coils, similar in physical size but with different wire diameters and numbers of turns, were used for the emitter and sensor, respectively. The emitter had a smaller effective area due to the smaller number of turns but could handle larger currents due to the larger wire diameter which allowed it to produce the strong magnetic fields. A commercially available copper coil (DigiKey part N 732-11702-ND) having 85 turns with an outer radius of 2.6 mm, inner radius of 1.7 mm, and height of 3.3 mm was used as the emitter. To prevent the overheating and melting of the emitter for the large currents used it had to be cooled by blowing dry liquid nitrogen vapor. The liquid nitrogen vapor was generated by running nitrogen gas through liquid nitrogen contained in an insulated tank.

The sensor had a larger effective area due to the larger number of turns even though the physical size remained similar (outer radius of 2.7 mm, inner radius of 1.6 mm and height of 5 mm). The sensor coil was fabricated using 40 AWG copper wire (Remington Inc., MW 79-C) wound on a ferrite core (DigiKey part N 1934-1347-ND). The wire was wound tightly on a 5 mm long ferrite rod, ensuring each turn was tight, circular and planar. Very circular and planar windings of the wire are necessary to achieve high sensitivity and good alignment of the sensor coil. The resulting coil, with 500 turns, allowed detection of nT magnetic fields.

Calibration. – Now we discuss the calibration of the emitter and sensor effective areas, A_{eff}, through generation

of static magnetic field and measurement of the dipole moments of the emitter and sensor coils by using a calibrated Gaussmeter (Lakeshore Model 460). A DC current, I, was applied to the coil, and the generated magnetic field $B(z)$ was measured at different heights z along the vertical axis of the dipole using the Gaussmeter. To cancel the background magnetic field, at each value of z, the average of the two measurements with currents running clockwise and counterclockwise were used. The data at large z were fit to the theoretical axial magnetic field $B(z)$ for the ideal dipole using the equation [51]

$$B(z) = \frac{\mu_0}{2\pi}\frac{m_0}{z^3} \tag{6}$$

and corresponding magnetic dipole moments m_0 of the coils were found. From the dipole moments, for the current I the effective areas A_{eff} of the coils were calculated from $A_{\text{eff}} = m_0/I$. As a result, A_{eff} of the emitter and sensor were found to be $1.40 \times 10^{-3}\,\text{m}^2$ and $2.49 \times 10^{-2}\,\text{m}^2$, respectively.

Experimental procedure. – Special attention was paid to the background noise and its reduction. Given the sensitivity of the measurements and the low level of the magnetic fields being detected, even small amounts of noise could significantly affect the results. To minimize background noise, all components, including the coils, leads, holders, cables, and connectors, were properly grounded. The wires connecting the coils were tightly braided to prevent the generation or being affected by stray magnetic fields. Cables connecting the power source and Lock-In Amplifier were enclosed in stainless-steel tubes and securely fixed. The background noise value without the copper plate was then measured on the Lock-In Amplifier and subtracted from all measurements. This value was 21.21 nV and found to be independent of frequency.

Then the emitter and sensor positioning and alignment were performed. For this purpose, both the emitter and sensor coils were mounted on the ends of a 28 cm long ceramic tubes with a diameter of 9 mm. The ceramic tube was held by a xyz micrometer controlled positioning stage fixed to the optical table. The coils were positioned at least 30 cm above the optical table. Care was taken to remove any metallic reflecting objects near the experiment. First the coils were placed next to each other with their axes aligned and parallel to the plane of the optical table. Next the current was turned on to the emitter at the experimental frequency $f_d = \omega_d/(2\pi)$. For the emitter current the reference sine output of the Lock-In Amplifier was amplified using a EuroPower EP2000 power current amplifier and applied to the emitter coil. An ammeter (Agilent 34411A Digital Multimeter) was used to measure the current flowing through the emitter coil. As noted above, the emitter coil was cooled by blowing dry liquid nitrogen vapor to prevent its melting.

Then the phase reading on the Lock-In Amplifier was set to zero. Next the axis of the emitter coil was rotated by 90 degrees to be perpendicular to the plane of the table. By using flat plastic blocks on top of the optical table, the emitter coil axis was confirmed to be perpendicular to the optical table. Next small corrections to the sensor coil axis orientation were done to make the measured emf signal zero. This confirmed that the axis of the sensor was perpendicular to that of the emitter. The sensor coil was moved to the needed x distance from the emitter using the x-axis micrometer. The perpendicular orientation of the sensor axis was further checked by minor adjustments to its plane by zeroing the sensor emf signal. Then, a 2.5 cm thick, $30 \times 30\,\text{cm}^2$ copper plate (Alloy 101: Oxygen-Free Electronic, Sequoia Brass and Copper Inc.) was placed on the optical table at a distance h below the coil centers. The distance h to the copper plate was changed by using flat insulating plastic blocks on the optical table below the copper plate. This ensures that the copper plate is parallel to the optical table and the sensor axis while being perpendicular to the emitter axis. This was also confirmed by sliding a perpendicular L scale.

The data collection was made as follows. Prior to the experiment, the copper plate was cleaned with acetic acid, acetone, and methanol to remove oxide layers and organic contaminants. It was then electrically grounded to the universal ground. An AC current with a desired frequency and amplitude was supplied to the emitter coil. The magnitude and phase angle of the induced emf on the sensor coil, caused by the lateral component of the reflected magnetic field from the copper plate, were measured using the Lock-In Amplifier (SR830 DSP). The time constant for signal averaging on the Lock-In Amplifier was set to 1 s. To minimize noise, the Lock-in's inbuilt sync filter was used, and the dynamic reserve was set to "low noise." The system was allowed to equilibrate for 2 minutes before taking the first measurement. A total of 10 measurements were recorded at 15-second intervals for both magnitude and phase angle of the induced emf.

The copper plate was then moved to a different distance h below the coils while maintaining the same distance x between the coils. After each height adjustment, the copper plate was removed to confirm the emitter and sensor coil orientations were perpendicular to each other and that there was no additional background noise signal. Once all measurements were taken for a set of heights h at a particular current frequency f_d, the process was repeated for other frequencies. Next, the distance between the coils x was changed to another desired value using the micrometer, and measurements were repeated for different emitter-sensor heights h above the plate and current frequencies f_d. The experiment was conducted for inter-coil distances x = 42, 46, 50, 54, 58, and 62 mm, and plate-coil heights h = 42, 50, and 62 mm, at current frequencies f_d = 12, 15, 20, 25, and 50 Hz. The measured emf, $\mathcal{E}$, was converted to the lateral magnetic field B_x using $B_x = \mathcal{E}/(2\pi i f_d A_{\text{eff}})$ [51], where A_{eff} is the effective area of the sensor coil discussed above and f_d is the frequency of the signal in Hz.

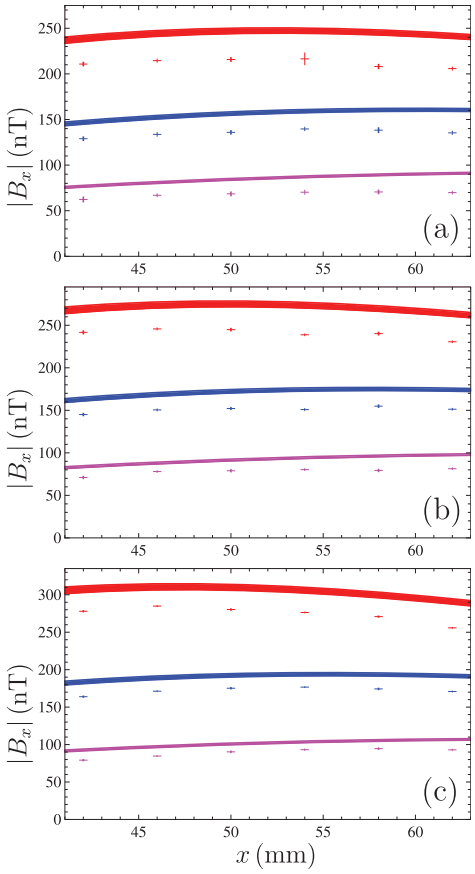

Fig. 2: The mean magnitude of the lateral component of oscillating magnetic field reflected from a copper plate is shown by crosses as a function of separation from the emitter for the oscillation frequencies (a) 15 Hz, (b) 25 Hz, and (c) 50 Hz. The theoretical bands for the absolute value of the reflected field are computed at the same frequencies using the dielectric permittivity of the Drude model. The bands and the corresponding sets of crosses counted from top to bottom are plotted for the emitter heights of 42, 50, and 62 mm.

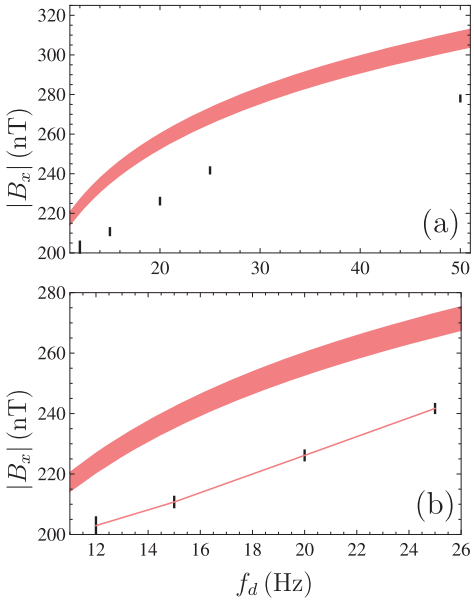

Fig. 3: The mean magnitude of the lateral component of oscillating magnetic field reflected from a copper plate is shown by crosses as a function of the emitter frequency at the height $h = 42$ mm and separation from the emitter $x = 42$ mm. The theoretical band for the absolute value of the reflected field is computed under the same conditions using the dielectric permittivity of the Drude model within the frequency regions (a) from 11 to 51 Hz and (b) from 10 to 26 Hz.

The mean measured values of $|B_x|$ are shown by crosses in fig. 2 as the function of separation between the emitter and sensor for f_d equal to (a) 15 Hz, (b) 25 Hz, and (c) 50 Hz. The vertical arms of the crosses indicate the random errors in the mean lateral magnetic field which were found at the 67% confidence level. The systematic errors, which are due to the error from sensor coil emf measurement, the error from measurement of frequency, and the error from measurement of the effective area of sensor coil, are much less than the random error. The horizontal arms of the crosses show the error in measuring separations with the Vernier calipers, $\Delta x = 0.2$ mm.

Comparison with theory. – The theoretical values of the lateral magnetic field in the experimental configuration were computed with eq. (5) using the dielectric permittivity of the Drude model (1) and the reflection coefficient (4). Note that the presence of hard plastic blocks under the copper plate does not influence the obtained results. The value of the plasma frequency for Cu, $\omega_p = 1.12 \times 10^{16}$ rad/s [52], has been used. The value of the relaxation parameter, $\gamma = 1.93 \times 10^{13}$ rad/s, was determined from the conductivity of the Cu sample, $\sigma = 5.77 \times 10^7$ S/m, indicated by the manufacturer. The error in the theoretical values is mostly determined by the errors in x and h, $\Delta x = \Delta h = 0.2$ mm, whereas the error in the value of γ was found to be negligible. The theoretical predictions for the magnitude of the lateral magnetic field $|B_x|$ are presented as bands with the widths equal to twice the total theoretical error. To find the width of the theoretical band, for each set of the parameters, the computation was repeated with the values $x \pm \Delta x$, $h \pm \Delta h$, and the smallest and largest of the four values were selected.

The theoretical bands obtained for the magnitude of magnetic field reflected from a copper plate are shown in fig. 2(a), (b), (c) as a function of separation from the emitter for different values of the dipole oscillation frequency (a) $f_d = 15$ Hz, (b) $f_d = 25$ Hz, and (c) $f_d = 50$ Hz. The bands counted from top to bottom are plotted for the emitter magnetic dipole heights above the copper plate $h = 42$, 50, and 62 mm.

In fig. 3(a), the theoretical band for the magnitude of the reflected magnetic field is shown as a function of the dipole oscillation frequency. The measured values for the magnitude of the reflected magnetic field are shown by crosses as in fig. 2. For better visualization, the region of

frequencies from 10 to 26 Hz is reproduced on an enlarged scale in fig. 3(b).

From figs. 2 and 3 it can be observed that for all the three frequencies of the emitted magnetic field, heights above the copper plate, and for all separation distances to the observation point from 42 to 62 mm the theoretical predictions for the magnitude of the lateral reflected magnetic field are excluded by the measurement data. Furthermore, the dependence of the measurement data on frequency shown in fig. 3(b) is qualitatively different from that predicted by the theory. What this means is that the Drude model provides an incomplete representation of the response of metals to low-frequency s-polarized evanescent waves.

Conclusions and discussion. – The performed experimental test for the completeness of the Drude model in the area of s-polarized evanescent waves is entirely classical. By contrast, the Casimir effect at short separations currently tested experimentally is a quantum phenomenon. The lateral component of magnetic field reflected from metallic plate is completely determined by the s-polarized evanescent waves, *i.e.*, by the region where the Drude model lacks experimental confirmation. In the case of the Casimir force, the contribution of s-polarized evanescent waves is responsible for the disagreement between the measurement data and theoretical predictions using the Drude model. However, it is important to note that for the s-polarized evanescent waves contribution using the Drude model the values of the characteristic parameter $ck_\perp/\omega$ giving the dominant fraction of the lateral component of magnetic field and that responsible for the disagreement in the measurements of the Casimir force are different. Thus, at the typical height of $h = 5\,\text{cm}$, a 95% contribution to the lateral magnetic field coming from the s-polarized evanescent waves is given by the interval $ck_\perp/\omega_d$ from 10^7 to 10^9. At the typical separation of 500 nm between the interacting surfaces, the 95% of the s-polarized evanescent waves contribution to the Casimir force comes from the interval $ck_\perp/\omega$ from 10^2 to 10^4. In both cases, the strongly evanescent waves are responsible for the disagreement between experiment and theory, but there is a five orders of magnitude difference in their regions of contribution.

Given the above, it appears that the understanding of the response of metals to s-polarized evanescent waves is not complete and some modifications in the permittivity given by the Drude model (1) might be necessary. The case of graphene, whose low-frequency dielectric response is found from the first principles of quantum field theory [53–57] and confirmed by the experimental data of the Casimir force measurements in graphene systems [58,59], suggests that this dielectric function should be spatially nonlocal and possess a double pole at zero frequency [60]. This may explain why the Casimir force experiments [6,17–28] are in agreement with theoretical predictions of the Lifshitz theory if the low-frequency response of metals is described by the plasma model (*i.e.*, by eq. (1) with $\gamma = 0$), which does not take dissipation into account and should not be applicable at low frequencies. Mention should be made that the magnitudes of the reflected lateral magnetic field computed with eq. (5) using the plasma model lie 26% to 93% higher depending on the values of f_d, x and h than the theoretical bands in figs. 2 and 3, *i.e.*, they are in even stronger disagreement with the measurement data than those found using the Drude model. This means that a successful use of the plasma model for calculation of the Casimir force is merely due to its fortuitous proximity to the true dielectric function in the region of parameters characteristic for the Casimir effect.

The search for the complete dielectric response of metals to the s-polarized evanescent waves in different physical systems is currently under active investigation (see, for instance, [61–68]). Future work will enable the development of the spatially nonlocal permittivity that will fully describe the dielectric response of metals to both propagating and evanescent waves of any polarization. The development of such a permittivity will be performed starting from the first principles of quantum electrodynamics along with the measurement data of many experimental tests including this experiment and experiments on measuring the Casimir force. The resolution of this problem will impact research in the areas of nanophotonics, optical quantum computing on a chip, near-field optical microscopy and its applications to overcoming the standard resolution limit, physics of total internal reflection and surface plasmon polaritons, to say nothing of the Casimir effect and related quantum phenomena of atomic friction and radiation heat transfer.

* * *

We are grateful to V. B. Svetovoy for useful discussions. The work of MD and UM was partially supported by the NSF Grant No. PHY-2012201. The work of GLK and VMM was supported by the State Assignment for Basic Research (project FSEG-2023-0016).

Data availability statement: All data that support the findings of this study are included within the article (and any supplementary files).

REFERENCES

[1] Ashcroft N. W. and Mermin N. D., *Solid State Physics* (Saunders College Publishing, San Diego) 1976.
[2] Casimir H. B. G., *Proc K. Ned. Akad. Wet. B*, **51** (1948) 793.
[3] Lifshitz E. M., *Zh. Eksp. Teor. Fiz.*, **29** (1955) 94; *Sov. Phys. JETP*, **2** (1956) 73.
[4] Dzyaloshinskii I. E. *et al.*, *Usp. Fiz. Nauk*, **73** (1961) 381; *Adv. Phys.*, **10** (1961) 165.

[5] Lifshitz E. M. and Pitaevskii L. P., *Statistical Physics, Part II* (Pergamon, Oxford) 1980.
[6] Decca R. S. *et al.*, *Phys. Rev. D*, **68** (2003) 116003.
[7] Mostepanenko V. M. and Trunov N. N., *The Casimir Effect and Its Applications* (Clarendon Press, Oxford) 1997.
[8] Milton K. A., *The Casimir Effect: Physical Manifestations of Zero-Point Energy* (World Scientific, Singapore) 2001.
[9] Buhmann S. Y., *Dispersion Forces*, Vols. **I**, **II** (Springer, Berlin) 2012.
[10] Bordag M. *et al.*, *Advances in the Casimir Effect* (Oxford University Press, Oxford) 2015.
[11] Sernelius Bo E., *Fundamentals of van der Waals and Casimir Interactions* (Springer, Cham) 2018.
[12] Klimchitskaya G. L. *et al.*, *Rev. Mod. Phys.*, **81** (2009) 1827.
[13] French R. H. *et al.*, *Rev. Mod. Phys.*, **82** (2010) 1887.
[14] Capasso F. and Johnson S. G., *Nat. Photon.*, **5** (2011) 211.
[15] Woods L. M. *et al.*, *Rev. Mod. Phys.*, **88** (2016) 045003.
[16] Palasantzas G. *et al.*, *Appl. Phys. Lett.*, **117** (2020) 120501.
[17] Decca R. S. *et al.*, *Ann. Phys. (N.Y.)*, **318** (2005) 37.
[18] Decca R. S. *et al.*, *Phys. Rev. D*, **75** (2007) 077101.
[19] Decca R. S. *et al.*, *Eur. Phys. J. C*, **51** (2007) 963.
[20] Bimonte G. *et al.*, *Phys. Rev. B*, **93** (2016) 184434.
[21] Bimonte G. *et al.*, *Universe*, **7** (2021) 93.
[22] Chang C.-C. *et al.*, *Phys. Rev. B*, **85** (2012) 165443.
[23] Banishev A. A. *et al.*, *Phys. Rev. B*, **85** (2012) 195422.
[24] Banishev A. A. *et al.*, *Phys. Rev. Lett.*, **110** (2013) 137401.
[25] Banishev A. A. *et al.*, *Phys. Rev. B*, **88** (2013) 155410.
[26] Xu J. *et al.*, *Phys. Rev. A*, **97** (2018) 032501.
[27] Liu M. *et al.*, *Phys. Rev. B*, **100** (2019) 081406(R).
[28] Liu M. *et al.*, *Phys. Rev. A*, **100** (2019) 052511.
[29] Klimchitskaya G. L. *et al.*, *Phys. Rev. B*, **101** (2020) 075418.
[30] Sushkov A. O. *et al.*, *Nat. Phys.*, **7** (2011) 230.
[31] Klimchitskaya G. L. *et al.*, *Int. J. Mod. Phys. A*, **26** (2011) 3918.
[32] Bezerra V. B. *et al.*, *Phys. Rev. B*, **83** (2011) 075417.
[33] Torgerson J. R. and Lamoreaux S. K., *Phys. Rev. E*, **70** (2004) 047102.
[34] Bimonte G., *Phys. Rev. E*, **73** (2006) 048101.
[35] Intravaia F. and Henkel C., *Phys. Rev. Lett.*, **103** (2009) 130405.
[36] Intravaia F. *et al.*, *Phys. Rev. A*, **82** (2010) 032504.
[37] Svetovoy V. B. and Esquivel R., *J. Phys. A: Math. Gen.*, **39** (2006) 6777.
[38] Klimchitskaya G. L. and Mostepanenko V. M., *Physics*, **5** (2023) 952.
[39] Zhang J. *et al.*, *J. Phys. D: Appl. Phys.*, **45** (2012) 113001.
[40] Törmä P. and Barnes W. L., *Rep. Prog. Phys.*, **78** (2015) 013901.
[41] Greffet J.-J. and Carminati R., *Prog. Surf. Sci.*, **56** (1997) 133.
[42] Aigouy L. *et al.*, *Opt. Lett.*, **24** (1999) 187.
[43] Hsu J. W. P., *Mater. Sci. Eng.: R: Rep.*, **33** (2001) 1.
[44] Sanjeev A. *et al.*, *Sci. Rep.*, **13** (2023) 15408.
[45] Brady J. J. *et al.*, *J. Opt. Soc. Am.*, **50** (1960) 1080.
[46] Zhu S. *et al.*, *Am. J. Phys.*, **54** (1986) 601.
[47] Van Rossum A. and Van Den Berg E., *J. Phys.: Conf. Ser.*, **1929** (2021) 012050.
[48] Klimchitskaya G. L. *et al.*, *EPL*, **139** (2022) 66001.
[49] Klimchitskaya G. L. *et al.*, *Universe*, **8** (2022) 574.
[50] Landau L. D. and Lifshitz E. M., *The Classical Theory of Fields* (Pergamon, Oxford) 1971.
[51] Jackson J. D., *Classical Electrodynamics* (Wiley, New York) 1999.
[52] Ordal M. A. *et al.*, *Appl. Opt.*, **24** (1985) 4493.
[53] Bordag M. *et al.*, *Phys. Rev. B*, **80** (2009) 245406.
[54] Fialkovsky I. V. *et al.*, *Phys. Rev. B*, **84** (2011) 035446.
[55] Bordag M. *et al.*, *Phys. Rev. D*, **91** (2015) 045037; **93** (2016) 089907(E).
[56] Bordag M. *et al.*, *Phys. Rev. B*, **93** (2016) 075414; **95** (2017) 119905(E).
[57] Bordag M. *et al.*, *Phys. Rev. D*, **109** (2024) 125014.
[58] Liu M. *et al.*, *Phys. Rev. Lett.*, **126** (2021) 206802.
[59] Liu M. *et al.*, *Phys. Rev. B*, **104** (2021) 085436.
[60] Klimchitskaya G. L. and Mostepanenko V. M., *Phys. Rev. D*, **107** (2023) 105007.
[61] Langsjoen L. S. *et al.*, *Phys. Rev. A*, **86** (2012) 010301(R).
[62] Klimchitskaya G. L. and Mostepanenko V. M., *Eur. Phys. J. C*, **80** (2020) 900.
[63] Klimchitskaya G. L. and Mostepanenko V. M., *Phys. Rev. D*, **104** (2021) 085001.
[64] Hannemann M. *et al.*, *Universe*, **7** (2021) 108.
[65] Loring R. F., *J. Phys. Chem. A*, **126** (2022) 6309.
[66] Henkel C., *Physics*, **6** (2024) 568.
[67] Klimchitskaya G. L. and Mostepanenko V. M., *Int. J. Mod. Phys. A*, **40** (2025) 2543005.
[68] Henkel C., *Int. J. Mod. Phys. A*, **40** (2025) 2543007.